Journal of Korean Powder Metallurgy Institute
Vol. 9, No. 6, 2002

Mechanically Driven Decomposition of Intermetallics

Young-Soon Kwon, Hyun-Sik Kim and Konstantin B. Gerasimov*
Regional Research Center, ReMM, School of Materials Science and Engineering
University of Ulsan, Ulsan, 680-749, Korea
**Institute of Solid State Chemistry and Mechanochemistry, Kutateladze 18, Novosibirsk-128, 630128 Russia*
(Received 30 October 2002 ; Accepted form 5 December 2002)

Abstract Mechanically driven decomposition of intermetallics during mechanical milling(MM) was investigated. This process for Fe-Ge and Fe-Sn system was studied using conventional XRD, DSC, magnetization and alternative current susceptibility measurements.

Mechanical alloying and milling form products of the following composition (in sequence of increasing Ge content): α (α_1) bcc solid solution, α +β-phase ($Fe_{2-x}Ge$), β-phase, β + FeGe(B20), FeGe(B20), FeGe(B20) + $FeGe_2$, $FeGe_2$, $FeGe_2$ + Ge, Ge. Incongruently melting intermetallics Fe_6Ge_5 and Fe_2Ge_3 decompose under milling. Fe_6Ge_5 produces mixture of â-phase and FeGe(B20), Fe_2Ge_3 produces mixture of FeGe(B20) and $FeGe_2$ phases. These facts are in good agreement with the model that implies local melting as a mechanism of new phase formation during mechanical alloying. Stability of FeGe(B20) phase, which is also incongruently melting compound, is explained as a result of highest density of this phase in Fe-Ge system.

Under mechanical milling (MM) in planetary ball mill, FeSn intermetallic decomposes with formation Fe_5Sn_3 and $FeSn_2$ phases, which have the biggest density among the phases of Fe-Sn system. If decomposition degree of FeSn is relatively small (<60%), milled powder shows superparamagnetic behavior at room temperature. For this case, magnetization curves can be fitted by superposition of two Langevin functions. Particle sizes for ferromagnetic Fe_5Sn_3 phase determined from fitting parameters are in good agreement with crystalline sizes determined from XRD data and remain approximately changeless during MM. The decomposition of FeSn is attributed to the effects of local temperature and local pressure produced by ball collisions.

Keywords: Mechanical Milling, Intermetallics, Mechanical induced decomposition, DSC

1. Introduction

Mechanically driven decomposition of intermetallic compounds is, probably, the most inscrutable among other phenomena observed for mechanical milling (MM). Indeed, why the same condition of milling leads in some cases to mixing of initially heterogeneous powder blends down to the atomic level with formation single solid phase, and in other cases to demixing of single solid phase with formation of heterogeneous blends.

P.I. Loeff and H. Bakker were the first who found decomposition of La-based intermetallics for high-energy ball milling.[1] According their data, these intermetallics decomposed into f.c.c. β-lanthanum and other elemental components. However, further deeper inspection showed that f.c.c. phase was not pure lanthanum but LaN, which had exactly the same lattice parameter as f.c.c. lanthanum.[2] In this case, decomposition turns up a selective oxidation reaction. The reason of decomposition of intermmetallics in Zr-Co and Ti-Cu systems in Ref. 3, after milling in high-energy planetary mill may be similar. Either Zr_3Co or $TiCu_4$ phase were always observed in decomposition products in this work; and these phases are stabilized by oxygen.

However, there are other examples, which are not simply explained by the contamination effects. Decomposition of $Nd_2Fe_{14}B$ and related compounds during mechanical milling, first observed by T. Alonso *et al.*[4], was reproduced in many other studies concerning synthesis of nanocomposite magnets. The

work on the studies of a milled Sm_2Fe_{17} compound indicated that Sm_2Fe_{17} decomposes into a mixture of an amorphous and α-Fe phase.[5] Decomposition of FeSn with formation of $FeSn_2$ and Fe_5Sn_3 was observed for mechanical milling.[6,7] S.L. Tang *et al.*[8] observed decomposition of $NdFe_{11}Ti$ compound firstly with formation of a mixture of metastable $Nd(Fe,Ti)_7$ and α-Fe(Ti), and after that a mixture of an amorphous phase and supersaturated solid solution of Ti in Fe.

Although the technique of mechanical alloying (MA) has progressed to the industrial level, research efforts to elucidate the operative mechanisms underlying MA have been limited. It is only recently that the science of this processing technology has begun to be investigated.[9,10] Expanding the scope of practical application of MA gives rise to demand for a model that be able to predict results of MA for given system and particular operation conditions and give ideas on how the conditions are to be changed to reach desired result. Physical background of MA is rather sophisticated; it is contributed by set of concurrent processes of different nature, so "ab-initio" models although exist rely heavy on present parameter. When number of the parameters grows model quickly loose its predicting ability.

In our opinion, satisfactory model of MA may be obtained from investigating results of MA in some model systems rather than attempting to synthesize MA from elementary acts. Such approach allows to reveal integral principles that characterize MA. One of such principles is hypothesis of local melting. We believe that this a hypothesis is fruitful approach for describing and understanding MA in many cases. However some investigators query possibility of temperature rise enough for melting, these conclusions follow from estimations of a temperature rise caused by mechanical energy dissipation during ball collisions.[11] Problem of these estimations is that the same amount of energy dissipated in enough small volume may produce arbitrary high temperature rise. While the energy may be estimated relatively credible, assumptions on the volume are inconclusive. So only experimental investigations may make conclusion on possibility of local melting.

2. Experimental

As a contamination by non-metal impurities may substantially change the resulting phase composition, a special care was taken to minimize the amount of oxygen found in specimen being treated. The main channels by which oxygen gets into the MA product are surface oxides and oxygen caught from atmosphere during the treatment in mill.

To reduce contamination associated with the surface, we did not use intentionally the fine dispersed powders. Coarse powders of Fe(99.9% purity), Ge(semiconductor grade) and Sn(99.99%) powder were used.

To get rid of contamination during mechanical alloying, the mechanical treatment was carried out in inert atmosphere. AGO-2 planetary ball mill was used for the treatment. This mill has two vials cooled during operation by running water. The vials have 150 cm^3 capacity and inner radius of 3.0 cm. The design of the vials allowed pumping and subsequent filling with gases up to pressure of 1.0 MPa. Hydrogen or argon with pressure of 0.5 MPa was used as atmosphere in vials in this study.[13] The hardened steel balls used for experiments were 3, 5.5, 7.5 and 9.5 mm in diameter. The ball charge was approximately 200 g and the mass of the powders being treated was 10 g in each vial. The operation mode of mill was as follows: the planet carrier radius (distance from the mill axes to vial axes) was 5.2 cm, the rotation frequency of planet carrier was 630 rpm, centrifugal acceleration was 226.3 m/s^2 (23 g), the rotation frequency of the vials was 1290 rpm.

For preparation of intermetallic compounds powder blends of Fe-Ge system with corresponding compositions were initially milled for 30 min and after that annealed in inert atmosphere during some days.

Despite of special care an oxygen contamination could not be avoided. Some oxygen contamination appeared in specimen being treated due to oxygen dissolved in original components and that absorbed at surface. Additionally a treatment in steel vials inevitably brought a contamination by balls and vials, mainly by iron. In our case ball and vial wearing does not change the system (it remains binary) but may case shift in composition. To verify that the level of contamination is small enough, all products of alloying were subjected to long annealing (4 hours at 600°C).

For preparation of FeSn intermetallic compound proper amounts of elements were previously mechanically alloyed during 30 min under hydrogen or argon and after that annealed in furnace in inert atmosphere at 970 K during 10 h.

For phase analysis, X-ray powder diffraction was carried out using DRON-4 diffractometer equipped with Co target X-ray tube and a diffracted-beam monochromator. The Rietveld method was utilized to extract information on the crystalline structure of the samples after MM, using W. Kraus and G. Nolzeís Powder-Cell 2.3 software package.

The magnetic measurements were performed in a vibrating sample magnetometer using a maximum applied field of 17.3 kOe. The temperature dependences of the real part of the a.c. susceptibility were determined from measurements in a sinusoidal field with amplitude 0.2 Oe and frequency 1.47 kHz under purified argon atmosphere. Thermal analysis of the samples was performed using ISI differential scanning calorimeter DSC-550 under argon gas.

The contamination by balls and vials could not be avoided in this case, too. The usual procedure to check contamination was by annealing milled samples at 673 K during 2 hours under inert atmosphere to restore sample and to get back the original properties. We check both phase composition and magnetic properties. Since FeSn intermetallic has small homogeneity range and all the phases of Fe-Sn system with iron content higher than in FeSn are ferromagnetic,[15] the magnetic properties should be especially sensitive to iron contamination. The small magnetization of samples after annealing is a straight confirmation of negligible iron contamination.

3. Result and Discussion

3.1. Fe-Ge system

The viewpoint on MA as an inherently low-temperature solid-state process[10] is likely to be common. In contrast, the model of local melting considers that phase formation during MA takes place in small regions of high temperature originated due to local plastic deformation as a result of milling bodies collisions. This model is now much less popular. Nevertheless some results concerning MA may be explained in much more obvious way just by model of local melting. The system investigated in this work provides such cases.

If MA or mechanical milling (MM) is carried out for sufficient long time, the material being milled must reach state, in which phase composition does not change upon further treatment (if case of oscillations is excluded). If this steady state does not depend on initial state of product but is a function of element composition and milling conditions only, it represents equilibrium state resulted from dynamic balance of processes taking place at mechanical treatment. Indeed, it was observed in Ref. 3 and 16 that at the steady state the composition and the structure of the products of metallic blends alloying and mechanical milling of individual intermetallics of the same chemical composition are identical. Studying steady states observed at MA and MM may give important information about the nature of MA. From viewpoint of the model of local melting, the corresponding dynamic equilibrium is a result of concurrency of melting in points of impact (which means decomposition of solid compound) and phase formation in the melted regions. If material is being treated for a long time, each particle has chance to be melted, hence steady state should corres-pond to phase composition resulted from cooling melt of corresponding composition. The steady state should not depend on initial state of material, as phase formation occurs from liquid state. On the contrary, if MA is only a solid-state diffusion enhancement by its nature, its driving force is difference of thermodynamic po-tential between material in starting and steady states. Changing initial state obviously influences value of the driving force. In particular case if starting phase composition corresponds to thermodynamic equilibrium, the driving force seems to vanish. Choosing composition that must produce different results according to these models (usually this is related to existence of low-temperature phase) evidence in favor to either model can be obtained.

When investigating steady states one should obtain evidence that composition observed really represents equilibrium state but does not follow from low rate of processes taking place at MA. Using apparatus that provides high milling power ensures that steady state will be reached in reasonable time. For many compositions investigated in this paper different initial states (elemental blends and intermetalics) were used. Results indicate that in all cases two hours of treatment were enough to reach steady state. The phase composition of products at steady state is presented in upper part of Fig. 1 together with equilibrium phase diagram for Fe-Ge system.

3.1.1 Iron rich compositions

The MA of Fe-Ge blends of iron content less than 27at% and milling of hexagonal ε-Fe_3Ge and cubic ε'-

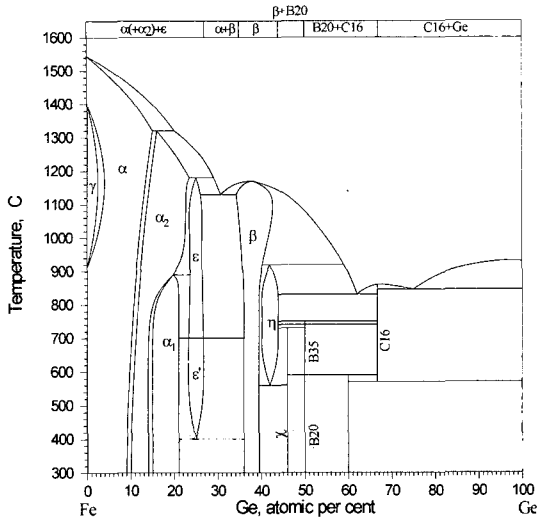

Fig. 1. Equilibrium phase diagram for Fe-Ge system. The map in the upper part reflects phase composition of the steady-state product for different chemical compositions.

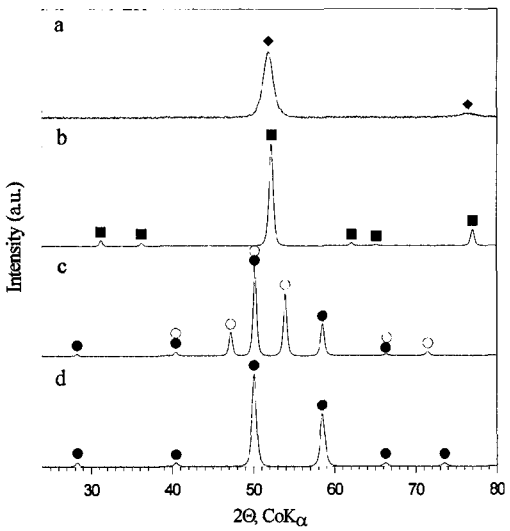

Fig. 2. XRD-patterns for $Fe_{75}Ge_{25}$ mechanical alloy: a. steady state after milling; b. after annealing at 500°C during 5 min; c. after annealing at 500°C during 1 h, d. after annealing at 500°C during 10 h. (◆)-reflections of α-phase, (■)-of DO_3, (●)-of cubic Fe_3Ge, (○)-of hexagonal Fe_3Ge.

Fe_3Ge intermetallics lead to the formation of bcc structures (Figure 2a). The lattice parameter increased with germanium concentration from 2.8664 A for pure iron to 2.898 A for $Fe_{75}Ge_{25}$ composition. The latest value is in good agreement with value of 2.90 A observed in Ref. 17 for bcc phase obtained by mechanical milling of Fe_3Ge intemetallic. As a few phases in this part of phase diagram are based on bcc lattice hence distinguish from each other by weak superlattice reflections, it is hard to reveal phase composition of the product using only XRD patterns of mechanical alloy. Short time annealing may enhance crystalline structure without substantial change of phase composition, giving chance to see superlattice reflections on XRD patterns. Figure 2b shows XRD pattern of mechanical alloy annealed for very short time at 773 K. The formation of transient DO_3 order is seen. More prolonged annealing lead to the mixture of high temperature hexagonal phase and equilibrium cubic phase (Fig. 2c). Finally single equilibrium ε'-Fe_3Ge observed after long annealing. Absence of ε'-Fe_3Ge decomposition during cooling obviously follows from kinetic difficulties.

If MA is a low-temperature process, MA of $Fe_{75}Ge_{25}$ composition should produce mixture of α_1 and β phase or ε'-Fe_3Ge (as its temperature of formation is enough low and may be observed as average temperature during treatment). Nevertheless, ε'-Fe_3Ge appears only after long annealing. Instead, sequence of high-temperature phases is observed in mechanical alloy. If phase formation takes place during cooling melted regions, the first phase precipitated from the melt of $Fe_{75}Ge_{25}$ composition is α_2. This conclusion is more close to experimental data.

3.1.2 Compositions with Ge content of 30-40%

Compositions $Fe_{70}Ge_{30}$, $Fe_{65}Ge_{35}$ and $Fe_{60}Ge_{40}$ were investigated. Mechanical alloying of $Fe_{70}Ge_{30}$ blend produces two-phase mixture of bcc phase and β-phase as a steady state product (Fig. 3). The bcc phase is similar to that observed as a product of MA of $Fe_{75}Ge_{25}$ composition, it undergoes same changes during annealing as $Fe_{75}Ge_{25}$ composition does. For $Fe_{65}Ge_{35}$ and $Fe_{60}Ge_{40}$ compositions single β-phase was observed.

β-phase is stable at low and high temperatures, it melts congruently. So it is expected as a product by both the models. However the models differ in the second phase observed in mechanical alloy of $Fe_{70}Ge_{30}$ composition is the same manner as in the case of $Fe_{75}Ge_{25}$ composition.

3.1.3 Composition corresponding to χ-Fe_6Ge_5

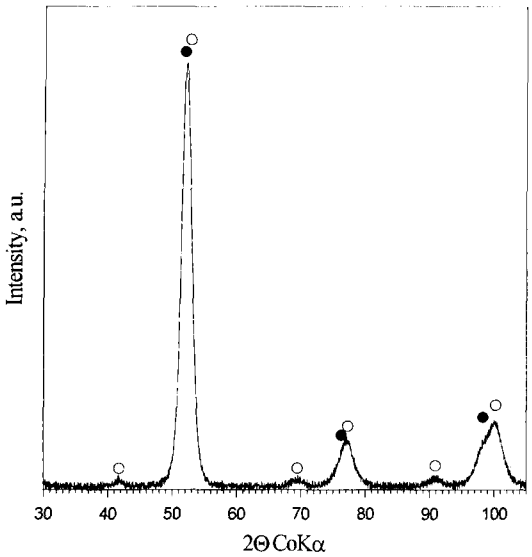

Fig. 3. XRD pattern for mechanical alloy $Fe_{70}Ge_{30}$. (●) - α-phase, (○) - β-phase.

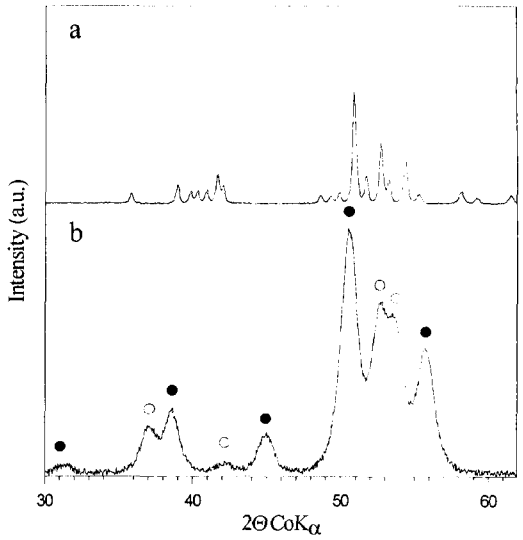

Fig. 4. XRD patterns for Fe_6Ge_5 intermetallic: a. before milling, b. after milling. (○) - reflection of β-phase, (●) - of FeGe(B20).

χ-Fe_6Ge_5 is a phase stable at low temperatures. This composition is interesting from viewpoint of model discrimination, as predictions of the model differ substantially. χ-Fe_6Ge_5 is expected as a result of MA by model of solid-state diffusion enhancement, but must decompose if phases are formed during cooling of melted regions.

Indeed, no trace of χ-Fe_6Ge_5 was detected in steady state products of MA elemental blends with content of Fe more than 45at%. Milling single χ-phase leads to decomposition, the product consists of mixture of β-phase and cubic FeGe (Fig. 4).

3.1.4 Composition $Fe_{50}Ge_{50}$

Elemental blend, low-temperature (cubic B20) FeGe and high-temperature (hexadecimal B35) FeGe were used as initial state. In all the cases product of MA consisted of cubic FeGe only. This fact seems to be in contradiction with model of local meltings, as cubic FeGe should decompose at high temperature, hence cannot form during cooling melt. Nevertheless this result also may be brought into accordance with the model of local meltings. Indeed, high local temperature results from plastic deformation, which in turn requires high local stress. The stress observed in material during MA is of order 1 GPa and may cause transformations of solids in high pressure polimorphs.[19] Hence, conditions of MA favor high-pressure modifications. Fig. 8 shows density intermediate phases in Fe-Ge system. Cubic modification of FeGe (B20) has the largest density of all phases in the system. Due to its high density this phase is expected to be more preferable under high-pressure observed during MA.

3.1.5 Ge-rich compositions

Two intermediate phases exist in this region, $FeGe_2$ and Fe_2Ge_3.[18] $FeGe_2$ melts congruently so it is expected to be product of MA in the model of local melting. However this compound is stable at high temperatures, hence low-temperature process would produce mixture of Fe_2Ge_3 with either Ge or FeGe depending on composition. MA of $Fe_{33}Ge_{67}$ blends and mechanical milling of $FeGe_2$ compound lead to same steady state. The XRD pattern of as milled samples shown on Figure 5a contain only broadened reflections of $FeGe_2$ (C16). DSC (Fig. 6) trace of heating these samples reveals exothermic effect at temperatures between 200 and 300°C and two endothermic peaks above 530°C. XRD patterns of the samples annealed at temperatures between exothermic effect and low-temperature exothermic effect contain reflections from germanium and from the Fe_2Ge_3-phase[18](Fig. 5b). In Ref. 18, it was shown that reflection from Fe_2Ge_3-phase may be satisfactory indexed. if this compound has a structure type of Ru_2Sn_3 with lattice parameters a = 5.59 A, c = 8.92 A. First endothermic

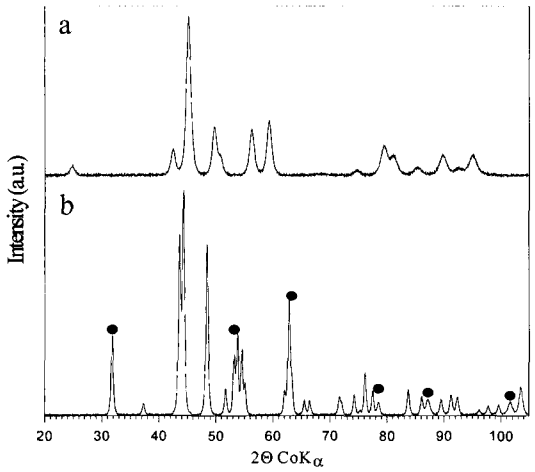

Fig. 5. XRD patterns of $Fe_{33}Ge_{67}$ mechanical alloy: a. steady state after milling, b. after milling and annealing at 450°C during 1 h. (●) - reflections of Ge.

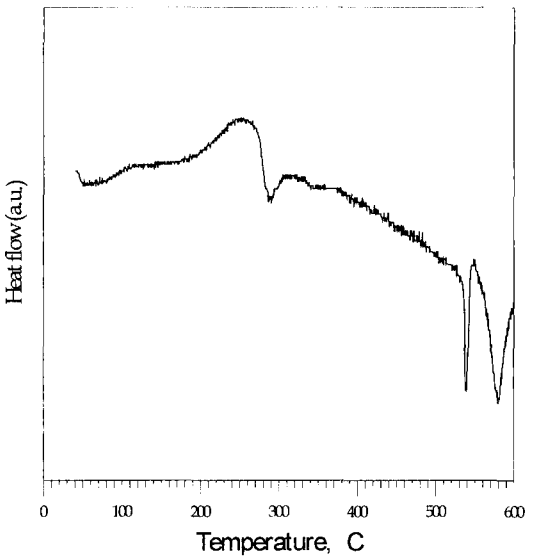

Fig. 6. DSC trace for $Fe_{33}Ge_{67}$ mechanical alloy.

effects correspond to the eutectioid transformation, when $FeGe_2$ begins to form. XRD patterns of the samples annealed to the temperature between the endothermic effects reveals reflection of both Fe_2Ge_3 and $FeGe_2$ phases, besides peaks from Ge. The second endothermic effect corresponds to the peritectoid transformation, in which Fe_2Ge_3 completely decomposed.

Fe_2Ge_3 is a low-temperature polymorph, according

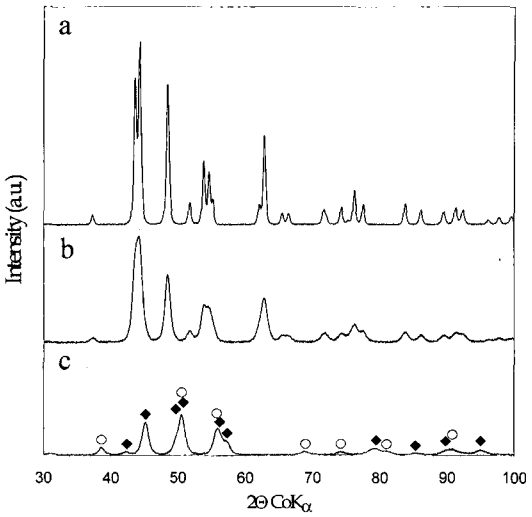

Fig. 7. XRD patterns of Fe_2Ge_3 intermetallic: a. before milling, b. after 6 min milling, c. after 40 min milling. (○) - reflections of FeGe(B20) phase, (◆) - from $FeGe_2$ phase.

to model of local melting it must decompose during grinding. On the contrary if MA were diffusion enhancement, Fe_2Ge_3 would be preferred product. Steady state of $Fe_{40}Ge_{60}$ MA as well as that of mechanical grinding of Fe_2Ge_3 represents mixture of $FeGe_2$ and cubic modification of FeGe (Fig. 7). Hence Fe_2Ge_3 is unstable during mechanical treatment, model of local melting again brings more realistic predictions.

3.2. Fe-Sn system

According to modern version of Fe-Sn phase diagram,[12] there are four intermetallic compounds in this system namely Fe_5Sn_3, Fe_3Sn_2, FeSn and $FeSn_2$. Fe_5Sn_3 and Fe_3Sn_2 phases are ferromagnetic, while FeSn and $FeSn_2$ are anti-ferromagnetic.[13] Decomposition of FeSn under MM with formation of $FeSn_2$ and one or several ferromagnetic phases was firstly observed in work.[5] More recently Mao et. al. also observed decomposition of FeSn due to MM and established that ferromagnetic phase was Fe_5Sn_3.[6,7]

Fig. 9 shows XRD patterns for initial FeSn intermetallic and for this intermetallic after MM together with results of Rietveld fitting in Powder Cell 2.3 program. It can be seen, that FeSn decomposed under MM into mixture of Fe_5Sn_3 and $FeSn_2$ phases. From the parameters of diffraction peaks fitting, the average grain size, which is dimension for coherent X-ray scattering, was determined. The grain sizes were approximately

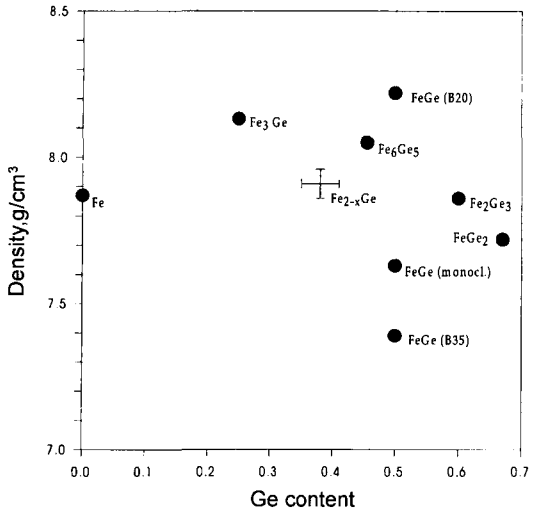

Fig. 8. Density of phases in Fe-Ge system.

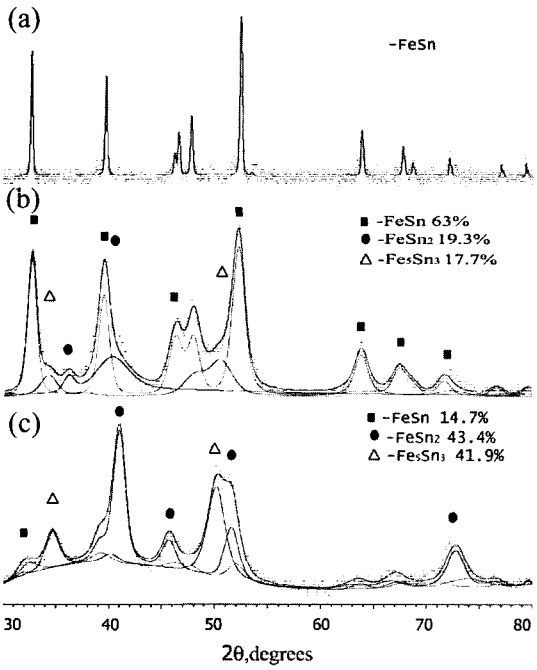

Fig. 9. Rietveld fitting of XRD patterns for FeSn intermetallic: (a) before MM, (b) after MM during 20 min with 5.5 mm balls, (c) after MM during 90 min with 5.5 mm balls.

equal to 10 nm for all phases, and only slightly changed with milling time and milling conditions. The particle sizes for milled powder were several tens μm.

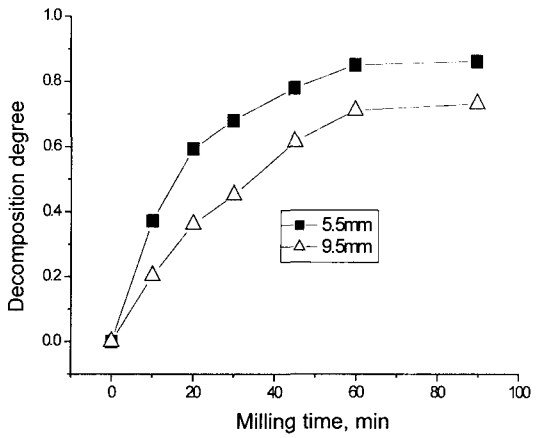

Fig. 10. Decomposition degree of FeSn as function of milling time for different diameters of milling balls.

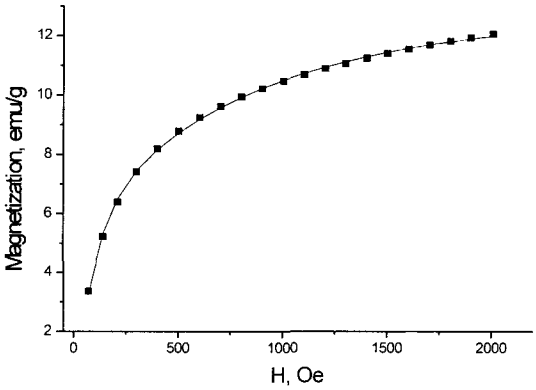

Fig. 11. Low-field magnetization curve of milled FeSn intermetallic with small decomposition degree. Squares represent experimental data; solid line is fitting by equation (1).

Decomposition degree of FeSn increased with milling time and reached a steady state for prolonged milling. From Fig. 10 one can see that decomposition of FeSn at this steady state is larger for smaller milling balls.

All phases in milled powders must possess superparamagnetic behavior at adequate high temperature due to small grain sizes. Small magnetic moment of anti-ferromagnetic FeSn and $FeSn_2$ particles was caused by an incomplete magnetic compensation. Fig. 11 shows typical room-temperature low-field magnetization curve of a sample milled from FeSn with relatively small decomposition degree. The magnetization shows no

hysteresis and magnetization and demagnetization curves coincide. As known,[15] the anhysteretic magnetization curves are always well described by superposition of a few Langevin functions characterized by different values of the magnetic moment. Such a fit allows one to obtain a value of the average magnetic moment in the system, as well as of the spread of the magnetic moment distribution. The particle sizes obtained using this procedure is consistent with results taken from different magnetic measurements[16] and from structural data analysis.[17] In our case, the magnetization curves for samples degree of FeSn less than 60% may be well fitted by sum of only two Langevin functions (Fig. 11):

$$M = N_1 M_1 \left[Coth\left(\frac{M_1 H}{kT}\right) - \frac{kT}{M_1 H} \right] + N_2 M_2 \left[Coth\left(\frac{M_2 H}{kT}\right) - \frac{kT}{M_2 H} \right] \quad (1)$$

where N_1 is the number and M_1 is the average magnetic moment of ferromagnetic (Fe_5Sn_3) particles; N_2 is the number and M_2 is the average magnetic moment of anti-ferromagnetic (FeSn and $FeSn_2$) particles; H is magnetic field; k is the Boltzmann constant and T is the absolute temperature.

N_1 value determined from fitting increased with milling time and magnetic moment of ferromagnetic particles M_1 changed only slightly in the range from 6.6×10^{-16} to 9.0×10^{-16} emu while decomposition degree of FeSn remained relatively small. From N_1 values, using 2.10 μ_B for magnetic moment of Fe atoms in Fe_5Sn_3 phase and 8.71 g/cm^3 for density of this phase,[13] we estimated an average particle volumes and particle sizes of this phase. For estimation the particles were implied having a cubic form and particle sizes were simply cubic root from particle volumes. Fig. 12 shows dependence of this particle size from milling time. The particle size remained approximately unchanged during first 30min of MM. Decrease of calculated particle size with further increase of milling time was really connected with magnetic interaction between particles in nanocomposite. Actually milled powders with decomposition degree of FeSn more than 60% (when milling time exceed 30 min) show hysteretic behavior (Fig. 13), and magnetization curves in this case cannot be well fitted by Eq. 1. These samples exhibit considerable magnetic viscosity: more than one hour time is needed to reach steady state magneti-

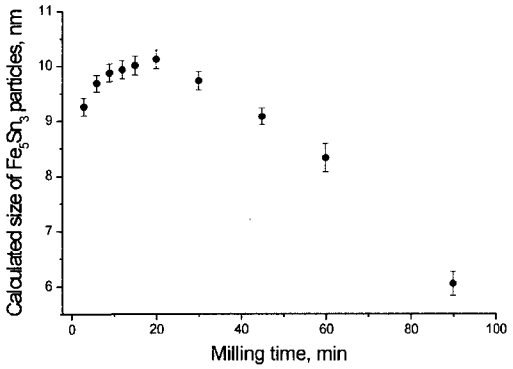

Fig. 12. Calculated sizes of Fe_5Sn_3 particles as function of milling time (5.5 mm balls).

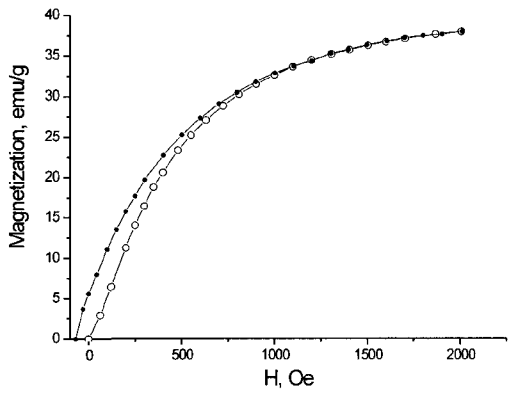

Fig. 13. Magnetization and demagnetization curves of FeSn after milling during 90 min with 5.5 mm balls showing hysteretic behavior.

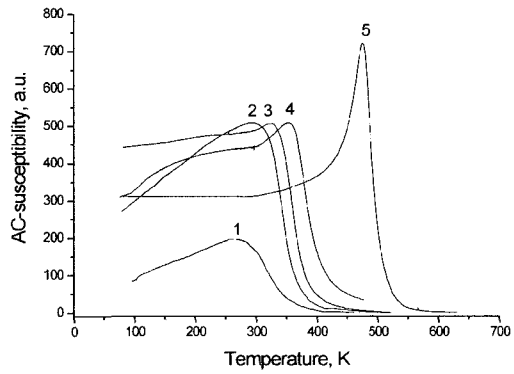

Fig. 14. Temperature dependences of the real part of the a.c. susceptibility of FeSn intermetallic patterns, milled with 5.5 mm balls during different time: 1. 6 min, 2. 20 min, 3. 30 min, 4. 45 min, 5. 90 min.

zation after a change of magnetic field.

Fig. 14 shows temperature dependences of real part of a.c. susceptibility for samples of milled FeSn. The powders with relatively small decomposition degree of FeSn (curves 1 and 2) exhibit broad maximum incident to individual particle magnetization freezing at the blocking temperature due to anisotropy energy barrier. The curve 5 is typical for Curie transition in ferromagnetic materials and curves 3 and 4 show intermediate type of behavior. So a.c. susceptibility data are in good agreement with emergence of hysteric features. While milled powders are mixtures of superparamagnetic particles of three phases, these nano-crystalline composites exhibit only one maximum on a.c. susceptibility curves.

Fig. 15 shows a typical DSC curve for milled powder. If milling time did not exceed 90 min, samples showed only negligible magnetization after heating above 700 K, the XRD pattern of the samples after heating did not differ from the XRD pattern of the initial FeSn intermetallic. For milling time, exceeded 90 min, this did not truth due to iron contamination from milling balls and vials.

Two explanation of the decomposition of FeSn intermetallic during MM are possible. First of them is based on an assumption that local temperature pulses due to ball collisions have relatively small value insufficient for local melting. In this case, the decomposition should be accounted for change of relative sta-bilities of phases of Fe-Sn system during MM due to preferential accumulation of defects in FeSn phase. The decomposition would occur by solid- state diffusion giving a gradual growth of both particle size and particle number with milling time for decomposition products at least for initial stage of MM.

The second explanation assumes that local melting is possible during impaction of powder. Several processes should be considered. All intermediate compounds of Fe-Sn system melt incongruently and can decompose under high temperature due to ball collisions. After collision, temperature of melted regions decreased rapidly and reverse processes of intermetallic formation become possible. All these processes must come into steady state after some time. As a result, the product of MM of FeSn must contain all the phases existing in Fe-Sn system. The amount of different phases may vary considerably, and only some of them may be detected in experiment. As ball collision generates not only high local temperature but also high local pressure, it is reasonably to expect that more dense phases should have bigger concentration in product of MM. Dachille and Roy[18] reported transformation of solids in more dense high-pressure polimorphs due to MM as early as 1960. Yao *et al.*[19] and Liu *et al.*[20] have recently shown that amorphous Fe-N alloy crystallized with formation dense high-pressure

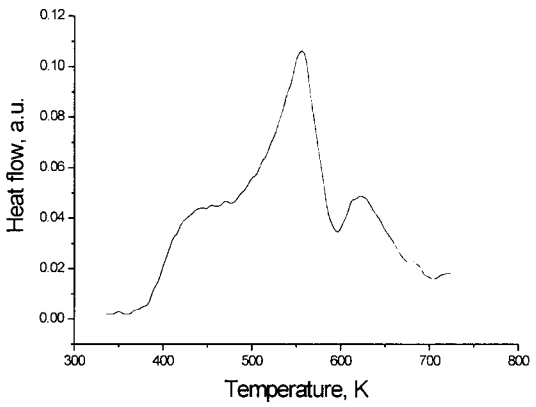

Fig. 15. Typical DSC trace for milled FeSn intermetallic. Heating rate is 10 K/min.

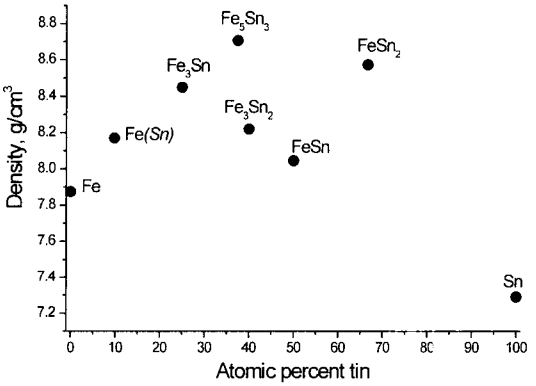

Fig. 16. Density of phases in Fe-Sn system, calculated from data of Ref. 9.

ε-Fe_xN phase during MM in a vibrating ball mill. The local pressure was estimated to be in the range 3.5-6.0 GPa and local temperature to be 650-1750K.[21] Fig. 16 shows density for phases in Fe-Sn system. The Fe_5Sn_3 and $FeSn_2$ phases prevailing in MM product have the largest density of all phases in the system.

The value and duration of local temperature pulses depend mostly on mechanical parameters of milling balls, their sizes, velocity and so forth (see Ref. 20 for

details) and should change only slightly with milling time. This means that, if decomposition of FeSn occurs due incongruent melting during impaction of powder, particle sizes of decomposition products would remain approximately changeless during MM process. Just such type of behavior was observed in this work. Using 10^{-7}-10^{-5} s for collision time and 10 nm for particle sizes and applying well-known relation $X^2 = 2Dt$, it is possible to estimate the diffusion coefficient for growth of Fe_5Sn_3 during powder impaction as $D \approx 5\times 10^{-6}$-$5\times 10^{-4} cm^2 s^{-1}$. This value is also typical for diffusion in a liquid state. Thus result obtained in this work supports the assumption that local melting is possible during MM process.

It is known, that multiphase ferromagnetic nanocomposites show only one Curie temperature T_c intermediate between T_c of constituent phases and increasing with fraction of the phase having bigger T_c[22]. We observed similar behavior for nanocomposite from two antiferromagnetic phases and one ferromagnetic phase produced by MM (T_c for Fe_5Sn_3 is equal 588 K, Neel temperatures for FeSn and $FeSn_2$ are 368 K and 380 K respectively[13]). Yelsukov et al.[23] also observed, that multiphase milled Fe-Sn alloys behaved in many aspect like a monophase system, exhibiting only one Tc which increased with iron content.

4. Conclusion

Mechanical alloying and milling of Fe-Ge system forms products of the following composition (in sequence of increasing Ge content): α (α_1) bcc solid solution, α+β-phase ($Fe_{2-x}Ge$), β-phase, β + FeGe (B20), FeGe(B20), FeGe(B20)+$FeGe_2$, $FeGe_2$, $FeGe_2$ +Ge, Ge. Incongruently melting intermetallics Fe_6Ge_5 and Fe_2Ge_3 decompose under milling. Fe_6Ge_5 produces mixture of α-phase and FeGe(B20), Fe_2Ge_3 produces mixture of FeGe(B20) and $FeGe_2$ phases. These facts are in good agreement with the model that implies local melting as a mechanism of new phase formation during mechanical alloying. Stability of FeGe(B20) phase, which is also incongruently melting compound, is explained as a result of highest density of this phase in Fe-Ge system.

Under mechanical milling (MM) in planetary ball mill FeSn intermetallic decomposes with formation Fe_5Sn_3 and $FeSn_2$ phases, which have the biggest density among the phases of Fe-Sn system. If decomposition degree of FeSn is relatively small (<60%), milled powder show superparamagnetic behavior at room temperature. For this case, magnetization curves can be fitted by superposition of two Langevin functions. Particle sizes for ferromagnetic Fe_5Sn_3 phase determined from fitting parameters are in good agreement with crystalline sizes determined from XRD data and remain approximately changeless during MM. The decomposition of FeSn is attributed to the effects of local temperature and local pressure produced by ball collisions.

Acknowledgements

This work has been supported by, the Korean Institute of S&T Evaluation and Planning (KISTEP), Program No. 02-3-20-8(invitation program), and has been also supported by the Korea Science and Engineering Foundation (KOSEF) through the ReMM at the University of Ulsan.

References

1. P. I. Loeff and H. Bakker: Europhys. Lett., **8** (1989) 35.
2. H. Bakker, G. F. Zhou and H. Yang: Progress Materials Sci., **39** (1995) 159.
3. K. B. Gerasimov, A. A. Gusev, E. Y. Ivanov and V. V. Boldyrev: J. Mater. Sci., **26** (1991) 2495.
4. T. Alonso, H. Yang, Y. Liu and P. G. McCormick: Appl. Phys. Lett., **60** (1992) 833.
5. K. B. Gerasimov and V. V. Boldyrev: Mater. Res. Bull., **31** (1996) 1297.
6. Ou Mao, R. A. Dunlap and J. R. Dahn: Solid State Ionics **118** (1999) 99.
7. Ou Mao and J. R. Dahn: J. Electrochem. Soc., **146** (1999) 414.
8. S. L. Tang, C. H. Wu, B. W. Wang, X. V. Jin, G. S. Li, B. Z. Ding and Y. C. Chuang: J. Magn. Magn. Mater., **188** (1998) 387.
9. C. Suryanarayana: Progress Mater. Sci., **46** (2001) 1.
10. C. Suryanarayana, E. Ivanov and V. V. Boldyrev: Mater. Sci. Eng., **A304-306** (2001) 151.
11. C. C. Koch: Int. J. Mechanochemistry and Mechanical Alloying, **1** (1994) 56.
12. K. C. Hari Kumar, P. Wollants and L. Delaey: Calphad, **20** (1996) 139.
13. G. Trumpy, E. Both, C. Diega-Mariadassou and P. Lecocq: Phys. Rev., **B2** (1970) 3477.
14. Y. -S. Kwon, K. B. Gerasimov and S. -K. Yoon: J. Alloys Comp. **346** (2002) 276.
15. P. Allia, M. Knobel, P. Tiberto and F. Vinai: Phys. Rev.

B52 (1995) 15398.
16. E. Agostinelli, P. Allia, R. Caciuffo, D. Fiorani, D. Rinaldi, A. M. Testa, P. Tiberto and F. Vinai: Mater. Sci. Forum **235-238** (1997) 705.
17. F. Vinai, P. Tiberto, A. Deriu, F. Malizia, M. Vittori-Antisari, M. Angiolini and J. S. Pedersen: Mater. Sci. Forum, **269-272** (1998) 339.
18. F. Dachille and R. Roy: Nature, 186 (1960) 34 and 89.
19. B.Yao, L. Liu, S. E. Liu, B. Z. Ding, W. H. Su and Y. Li: J. Non-Crystalline Solids, **277** (2000) 91.
20. L. Liu, S. Lun, S. E. Liu, X. D. Zhao, B. Yao and W. H. Su: J alloys Comp, **333** (2002) 202.
21. D. R. Maurice and T. H. Courtney: Metall. Transact, **21A** (1990) 289.
22. R. Skomski and D. J. Sellmyer: J. Appl. Phys. **87** (2000) 4756.
23. E. P. Yelsukov, E. V. Voronina, G. N. Konygin, V. A. Barinov, S. K. Godovikov, G. A. Dorofeev and A. V. Zagainov: J. Magn. Magn. Mater. **166** (1997) 334.